Moncho Esteve, IJ.; Palau-Salvador, G.; Brevis, W.; Vaas, M.; López Jiménez, PA. (2015). Numerical simulation of the hydrodynamics and turbulent mixing process in a drinking water storage tank. Journal of Hydraulic Research. 52(2):207-217. doi:10.1080/00221686.2014.989456.

Numerical simulation of the hydrodynamics and turbulent mixing process in a drinking water storage tank

IGNACIO J. MONCHO-ESTEVE, PhD Student, *Department of Rural and Agrifood Engineering, Hydraulic Division, Universitat Politècnica de València, Camino de Vera s/n, Valencia, Spain*

Email: igmones@doctor.upv.es (author for correspondence)

GUILLERMO PALAU-SALVADOR, Professor, *Department of Rural and Agrifood Engineering, Hydraulic Division, Universitat Politècnica de València, Camino de Vera s/n, Valencia, Spain*

Email: guipasal@agf.upv.es

WERNHER BREVIS (IAHR Member), Lecturer, *Department of Civil and Structural Engineering, The University of Sheffield, Mappin Street, Sheffield, UK*

Email: w.brevis@sheffield.ac.uk

MARKUS O. VAAS, Research assistant, *Institute for Hydromechanics, Karlsruhe Institute of Technology, Kaiserstr, 12, Karlsruhe, Germany*

Email: vaas@kit.edu

PETRA A. LÓPEZ-JIMÉNEZ (IAHR Member), Professor, *Hydraulic and Environmental Engineering Department, Universitat Politècnica de València, Camino de Vera s/n, Valencia, Spain*

Email: palopez@upv.es

Running Head: Numerical simulation of turbulent mixing

Numerical simulation of the hydrodynamics and turbulent mixing process in a drinking water storage tank

ABSTRACT

Jet-mixing and residence time in a rectangular water storage tank with a constant water level are investigated using tools of Computational Fluid Dynamics (CFD). A set of Unsteady Reynolds-Averaged Navier-Stokes (URANS) equations using a realisable k-ε model for different inlet configurations have been used. Numerical simulations were validated by means of experimental measurements. A saline inflow was simulated and the computed salinity in the outflow was compared with the measured values, with the aim of improving the tank performance based only on simple modifications of the inlet position and inflow rate. The results show that the URANS technique is able to adequately capture the experimental dilution curve measured at the outlet of the tank. The residence time is mainly influenced by advective transport. Modifications of the horizontal angle and Reynolds number of the inflow jet produce changes in the mixing characteristics when different performance indexes are compared.

Keywords: Computational Fluid Dynamics (CFD), drinking water tank, mixing parameters, turbulent mixing processes, Unsteady Reynolds-Average Navier-Stokes (URANS)

1 Introduction

Drinking water storage tanks are an important part of any water distribution system (WDS). One of their main functions is to store excess water, in the case of low demand, and also to provide extra volume when the WDS demand peaks. Although the study and modelling of these tanks are often simplified, their impact in maintaining an adequate water quality in the network is of paramount importance. Grayman et al. (2004) presented some guides in order to minimize problems in storage facilities resulting from the related phenomena of mixing and aging of WDS. Inadequate operation and design faults can cause different problems: harmful disinfectant residuals, growth of pathogens or problems with odours and discoloured water. Some examples of serious incidents due to ineffectual management of water tanks are documented by Boulos, Altman, Jarrige and Collevati (1994) and Clark, Goodrich and Wymer (1993). All these issues are linked to insufficient turnover and poor mixing. The complex flow developed within the tank, the presence of dead zones and hydraulic short-circuiting can produce long residence times T_r. This results in complex biological and chemical processes that can negatively affect water quality (Martínez-Solano, Iglesias-Rey, Gualtieri and López-Jiménez, 2010).

Previous water quality studies have assumed the tank as an ideal reactor, i.e. a continuous flow stirred tank reactor or a plug-flow reactor. However several works (Grayman

and Clark, 1993; Kennedy, Moegling, Sarikelle and Suravallop, 1993) have shown that the assumption of an ideal reactor is not always valid, which may lead to an underestimation of the water age in parts of the tank. Mau et al. (1995) carried out an explicit model for simulating water quality in tanks by considering five conceptual representations of multi-compartment models: a continuous flow stirred tank, a two-compartment tank, a three-compartment tank, a four-compartment tank and a plug-flow tank. Mixing behaviour and its effects on the water quality are considerably influenced by the turbulent flow patterns within the storage tanks.

Due to their high spatial and temporal resolutions, Computational Fluid Dynamics (CFD) methods can be seen as a valuable tool for the analysis and prediction of the water quality in storage tanks (Martinez-Solano, Iglesias-Rey, et al., 2010). Jet mixing in storage tanks has mostly been studied through intensive experimental procedures (Patwardhan, 2002), which normally result in empirical or statistical relationships between residence times and either geometrical or hydraulic parameters. Several authors, such as Metzger and Westrich (1978) or Maruyama and Mizushina (1982) have experimentally investigated the residence time as the main parameter for evaluating quality in water storage tanks; Rossman and Grayman (1999) conducted experiments on cylindrical tanks to study the effect of different factors such as the effect of source momentum on jet mixing. These attempts resulted in information about the general behaviour of the tank as a mixer, but they cannot be used to explain the physics of the underlying mixing process. Marek, Stoesser, Roberts, Weitbrecht and Jirka (2007) have pointed out that most of the research in flow and mixing processes in water storage tanks has been conducted by means of extensive and costly experiments. Tian and Roberts (2008) carried out extensive experiments to measure concentration fields over time in order to study the evolution of the jet-induced mixing processes in three types of storage tanks (ground level cylindrical, standpipe and ground level rectangular). They pointed out the convenience of performing CFD models, which can simulate three-dimensional circulations, to predict mixing and to design new infrastructures. Mahmood, Pimblett, Grace and Grayman (2005) demonstrated that CFD techniques are an effective tool for predicting mixing processes in water tanks, and that they are advisable when studying different operational conditions. Yeung (2001) studied flow distribution and water age in service reservoirs by using CFD and pointed out the advantages of CFD in these studies.

However, only a few CFD studies have approached the modelling of turbulent flow in drinking water storage tanks (Grayman et al., 1996; Hannoun and Boulos, 1997; Martínez-Solano, Mora-Rodríguez, Iglesias-Rey and López-Patiño, 2010; Palau-Salvador et al., 2007).

This paper presents the results of three-dimensional simulations of the flow and jet mixing in a jet-agitated drinking water storage tank with constant level. The simulations are carried out using the Unsteady Reynolds-Averaged Navier-Stokes (URANS) techniques in

order to simulate the flow and a point injection of conservative tracer into the tank. The numerical results are validated using experimental observations. In addition, two new configurations and different inflow rates are simulated and analysed to understand the role of the inflow geometrical characteristics of the inflow in the magnitude of the residence time. This methodology has been chosen to focus the experimental procedures on improving designs and optimising mixing capability.

2 Experimental setup and numerical method

2.1 Experimental case

A reservoir tank type was built for validating the numerical simulation. These sort of tanks can often be kept at a near-constant water level, acting as flow-through tanks with only limited differences between the inflow and outflow rate. The steady-state flow-through tank type was chosen specifically for this study for its ability to maintain a constant water level during operation. Thus, the effects of a strong unsteady flow caused by changes in the water volume in the tank were eliminated, and the experiment was focused on the effects of the internal flow structure coming from the jet inlet. Therefore, a 1:4 prototype laboratory model of a particular tank was built. This rectangular, open-top water storage tank with constant and equal in- and outflow discharge was built at the research laboratory of the Institute for Hydromechanics, Karlsruhe Institute of Technology (KIT). Figure 1 shows a schematic representation of the experimental tank. The dimensions are L = 2,050 mm, W = 1,525 mm, H = 760 mm (Fig. 1). As shown in Fig. 1, the inflow takes place through a 65 mm circular pipe (inlet section), which has a horizontal $2\pi/9$ rad bend (θ in Fig. 1), that ends in a 16.7 mm jet nozzle. The vertical inlet angle (Fig. 1) φ is 0 rad for this first configuration. Water leaves the tank through a 102 mm circular outlet pipe located close to the inlet pipe (Fig. 1). Other geometrical parameters shown in Fig. 1 are: A = 150 mm; B = 345 mm; C = 305 mm; D = 150 mm; E = 75 mm which represents distance of the inlet from L, distance of the outlet from L, length of inlet pipe into the tank, length of the inlet diffuser and height of the inlet pipe from the bottom respectively. In addition, the horizontal orientation of the inlet prevents direct interaction of the jet with the free surface, thus no surface waves are developed. The geometrical and flow conditions are specified in Table 1. U_{jet} (inlet velocity in the jet nozzle section) was equal to 1.90 ms^{-1} for the validation case. The densimetric Froude number, F_d, in the inflow has been estimated as indicated in Prešeren, Steinman, Širok and Bajcar (2013). This number is used for representing the relative importance of inertial and density gravity in terms of the influence of momentum and buoyancy flux when considering the difference in density between the inflow and the tank. In this case the densimetric Froude number was

estimated as $F_d = 0.703$.

In order to analyze the mixing process within the tank, a volume of 0.01 m^3 of brine with a salt concentration (C_{Salt}) of 50 gl^{-1} was injected (time $t = 0$ s) instead of the main inflow for 24 s. Salt concentration refers to dissolved salt content in fresh water: grams of dissolved salts (sodium (Na^+) and chloride (Cl^-) ions) in a litre of fresh water. When all the brine has been introduced into the tank, the inlet continues injecting fresh water constantly until the end of the experiment. The injection was carefully designed to avoid changes in the inflow discharge. The changes in conductivity of the water in both the inlet pipe and outlet pipe (~50 cm downstream of the tank exit) are recorded until inlet and outlet conductivity reach their value base again.

2.2 Numerical method

In this work, three-dimensional URANS simulations are performed using the Star-CCM+ commercial code (CD-Adapco Inc., 2010). The model is based on the mass and momentum conservation equations, neglecting temperature effects. The code is based on a finite-volume method (Veersteg and Malalasekera, 1998) for solving the Navier-Stokes equations. For the purpose of mass conservation, a standard pressure correction algorithm (SIMPLE) was used. For the turbulence closure the two equations realisable k-ε model (Shih, Liou, Shabbir, Yang and Zhu, 1994) was implemented.

A velocity inlet boundary condition was used in the inlet pipe. Slip condition was implemented in the walls. The free surface was modelled by a rigid-lid approximation, which is acceptable in the event of insignificant water surface deformation, a condition observed during the experimental work. A hybrid approach wall treatment was set for the near-wall modelling with a model for non-dimensional wall distance y^+ larger than 30 and resolving the boundary layer in the other cases. The initial conditions for the URANS were fixed by the steady state of the previous RANS solution. A time step of 0.5 s and a first-order upwind convection scheme were chosen for URANS solution with an implicit solver. This was a proper balance between accuracy and CPU time. A passive scalar model was used to simulate the brine injection (CD-Adapco Inc., 2010). Since the purpose of this work was to simulate the mixing processes of a tracer injection inside the tank (with NaCl as the passive scalar), the water density has been defined in each equation of the code, according to the salt concentration in each cell. This is possible in the definition of the physics conditions in the used software Star-CCM+. Consequently, the solution takes into account the slight differences in density when the salted water is injected.

Different kinds of grids were also developed and tested, achieving a grid independency with three different mesh sizes (Coarse ≈ 650,000 cells, Middle ≈ 950,000 cells

and Fine ≈ 1,700,000 cells). After preliminary simulations, no significant differences between the Middle and the Fine grids were found (see details of the final selected mesh in Fig. 2). This selection was based on a sensitivity analysis, which took into account comparison with the experiment, convergence criteria and simulation time. Therefore, the final grid used for the calculations was of 950,000 grid cells. The grid is finer near the walls and the grid size variation between cells is kept to a maximum geometrical increase of 4%.

2.3 Mixing parameters

Some mixing parameters were also considered and discussed in order to evaluate mixing efficiency. The parameters which were used in this work are listed as follows.

Mixing power

The mixing power was defined by Rushton and Oldshue (1953) as (1):

$$P = \Delta p Q_{in} \tag{1}$$

where P is the power, expressed in watts, Δp is the pressure drop between the outlet and the inlet (Pa) and Q_{in} is the flow rate (m^3s^{-1}) inside a mixer. This parameter can be used to estimate the power needed to achieve a proper mixing in the tank.

Velocity gradient

Metcalf and Eddy (1995) proposed the use of the velocity gradient as a method to quantify mixing in water engineering. The velocity gradient can be calculated as (2):

$$G = \sqrt{P/(\mu V_t)} \tag{2}$$

where V_t is the volume tank in m^3, P is the mixing power in watts and μ is the dynamic viscosity.

Dimensionless mixing time

The dimensionless mixing time was defined and used by Rossman and Grayman (1999). In this work, a dimensionless mixing time, as it was calculated by Tian and Roberts (2008), was obtained for all simulated cases. Tian and Roberts (2008) defined the mixing time t_m when the coefficient of variation (*COV*) fall to 10 %. The *COV* is defined for the simulations in each time as the standard deviation of the tracer concentration divided by the mean tracer concentration.

The dimensionless mixing time is defined, for a fixed value of *H/L*, as (3):

$$\tau_m = (t_m \, M^{1/2}) / V_t^{2/3} \quad (3)$$

where $M = U_{jet} \, Q_{in}$ is the momentum jet flux and V_t is the volume tank. Lower values of τ_m mean more efficient mixing in the tank.

Residence time distribution function

Residence time distribution function (*RTD*) was also obtained for all the simulations to obtain the short-circuit index θ_{10} (Teixeira and Siqueira, 2008) which gives a more quantitative description. The θ_{10} is the time needed by 10% of the tracer mass to reach the outlet section (t_{10}) divided by the theoretical retention time T_r. Van der Walt and Haarhoff (2000) proposed a four-tier hydraulic performance code for some indicators (where $\theta_{10} < 0.2$ means poor mixing due to tracer short-circuit).

2.4 Effect on the flow for different inlet parameters

In this paper, an analysis of the influence of the horizontal inlet orientation is presented after validation of the experimental case (T1_1 configuration). Two other simulated configurations, T2_1 and T3_1, are proposed, which are based on a modification of the horizontal angle of the jet nozzle (from 0 rad to 2π/9 rad). The influence of the Reynolds number in the jet nozzle section (R_{jet}) is also analysed. The R_{jet} varies between 9,860 and 88,736. Table 1 shows the different inlet parameters for the simulated tank.

3 Results and discussion

3.1 Calibrated model and validation

Figure 3 shows a comparison in a semi logarithmic graph, over the first 6,000 seconds, between experimental and simulated dilution curves in the outlet section of the tank for the T1_1 case (cross-section averaged values).

It is possible to observe the agreement between the experimental and the numerical results. In this case, the average absolute relative error is 2.81%, estimated along the residence time (T_r = 5,702 s). The beginning of the first peak of salt concentration, around 80 seconds after the injection, is reproduced fairly well by the simulation in time and intensity with an overestimation of 4% of the maximum peak of the outlet concentration (t =110 s). Between the first peak and until t = 350 s, the model reproduces a sinusoidal behaviour, with an amount of water with high salt concentration reaching the outlet via preferential paths, before it becomes completely mixed. Following this, C_{salt} reaches the value of 0.2 gl^{-1} and

after that decays until the concentration is zero again, which is reasonably well reproduced by the simulation.

3.2 Hydrodynamics and mixing process

Since the objective of this work is to simulate hydrodynamics and the mixing process inside the tank, the numerical results of the three-dimensional three-dimensional URANS for the T1_1 case are presented in this section.

The mean velocity vector module $\langle U \rangle = \sqrt{\langle u \rangle^2 + \langle w \rangle^2 + \langle v \rangle^2}$, where $\langle\ \rangle$ indicates time averaging, and *u*, *v*, and *w* are the instantaneous velocity components in the *X*, *Y*, and *Z* directions, respectively. Figure 4 shows $\langle U \rangle$ contours and the associated streamlines at several *Z* positions. This figure clearly shows the influence of the inlet on the topology of the flow patterns within the tank. Of note is the maximum velocity of the simulated flow due to the change of the diameter of the inlet pipe in the jet nozzle (from 65 mm to 16.7 mm). This reaches a peak centreline jet velocity of 2 ms^{-1} in the nozzle tip (location: *X* = 1.64 m; *Y* = 0.25 m) compared with the mean inlet velocity of 0.1256 ms^{-1} in the inlet section. Moreover, following the impingement of the jet against the corner on the opposite wall, the velocity considerably decreases reaching a velocity of about 0.027 ms^{-1}, which is about the magnitude of the mean tank velocity. The streamlines pattern suggests that there is neither strong nor clear shortcircuiting within the tank. The jet drives two large scale recirculating gyres. As shown in Fig. 4, these gyres can be observed at *Z*=0.111 m and *Z*=0.3 m, however these structures cannot be observed at higher positions. It is also possible to identify a relatively small cell near *X* = 1.1 m and *Y* = 1.5 m that rotates in the opposite direction.

The Peclet number *(*Pe*)* compares the advective and diffusive transport of a physical quantity, $Pe = (U\,l)/D_m$, where *U* and *l* are the velocity and length scales, and D_m the coefficient of molecular diffusion. A value of $1.489 \cdot 10^{-9}$ m^2s^{-1} is considered as the coefficient of the diffusion of the tracer. *U* is set to the local mean velocity magnitude in each cell, and *l* is equal to the size of the cell point. A value of the Peclet number greater than 1 indicates that advection is dominant over diffusion and a number less than 1 indicates that diffusion is dominant. Considering all the cells in the computed domain, the maximum Peclet number in the domain reaches the value of $6.6 \cdot 10^6$ and the minimum is $6.7 \cdot 10^3$. As it was expected, in a turbulent flow such as this, advective transport is much larger than molecular diffusion.

Figure 5 shows three iso-surfaces (1 gl^{-1}; 0.2 gl^{-1} and 0.1 gl^{-1}) of salt concentration at different times after the tracer injection. From the snapshots it can be seen that the mixing and dilution process, such as the dispersion pattern of the scalar in the tank, is clearly affected by the flow and seems to be predominantly advective. According to the first peak of the dilution

curve (Fig. 3), the 1.00 gl^{-1} iso-surface starts leaving the tank at snapshot t = 103 s. This indicates that an amount of tracer reaches the outlet via preferential paths, before it becomes completely mixed, due to the advection inside the tank.

The mixing efficiency within the tank was analysed using concentration histograms and the cumulative distribution. Figure 6 shows the tracer concentration histogram (main axis) and the cumulative distribution (second axis) for the T1_1 case at four different times. From these plots an increase in the average concentration and mixing over time can be observed (as dispersion decreases). Due to the low mixing levels at t = 23 s, the concentration reaches a magnitude close to 0.05 gl^{-1}. The tracer concentrations are more narrowly distributed shortly after injection and then become broader, and finally narrows as the tank becomes better-mixed. An increase in the dispersion of the tracer concentration can be observed from t = 23 s to t = 143 s. After this time the dispersion decreases with no significant changes in the average value. At t = 563 s, 99.44% of data are between 0.15 gl^{-1} and 0.25 gl^{-1}. These results show that homogeneous mixing conditions exist after about 9 minutes.

3.3 Sensitivity analysis of inlet parameters

This section presents a comparison of the results between the three studied configurations (T1_1, T2_1 and T3_1) and four different inflows for T1.

Inlet orientation

Figure 7 shows the three-dimensional streamlines (coloured by the mean velocity magnitude) for T1_1, T2_1 and T3_1 configurations. Although the flow is still three-dimensional and complex in all cases, with no evident dead-zones or clear short-circuiting, the streamlines are different. For the T1_1 case, it is possible to observe a significant reduction of velocity when the jet reaches the opposite corner. For the T2_1 simulation a large recirculation in the middle of the tank contrasts with the behaviour of the T1_1 case. The jet impinges on the opposite wall and splits into two main recirculation patterns. There is a low velocity zone between the two main flows characterised by a complex behaviour. Finally, for the T3_1 case, the jet impinges directly on the same corner of the opposite wall. In this case, the recirculation changes its rotational direction. There is again a low velocity zone in the middle of the tank with a chaotic and complex pattern. It was be observed that small changes in the inlet parameters of the water storage tank cause variations in the turbulence structures, which produce different mixing processes within the tank.

A comparison of mixing parameters between estimated in the three configurations with different horizontal inlet angles (T1_1, T2_1 and T3_1) is shown in Table 2. The mixing

power and the velocity gradient are in the same order of magnitude for all three cases. The results indicate that inlet changes can induce small changes on the salt dilution in the whole tank. Moreover, according to these parameters, a slightly better level of dilution is achieved for T2_1 (jet nozzle: $\theta = \pi/9$ rad); and on the other hand a lower level of dilution is observed for the T3_1 simulation (jet nozzle: $\theta = 0$ rad).

Table 2 also shows τ_m for the three inlet angles. These values are in the same order of magnitude as those obtained by Tian and Roberts (2008) in a rectangular tank, with a constant ratio H/L=0.29 and a single horizontal nozzle. The results also suggest better mixing capability for a horizontal orientation of $\pi/9$ rad in this specific position of the inflow (T2_1 simulation).

Table 2 shows the results of θ_{10} for the different horizontal angles (T1_1, T2_1 and T3_1 simulations). In all cases, the value are lower than 0.2, which means poor efficiency from a short-circuit point of view. This lower value is due to an amount of water with high salt concentration reaching the outlet via preferential paths, before it becomes completely mixed. This must be due to the advection of the flow in the tank. From the results and according to θ_{10}, it is possible to see that the horizontal modification of the nozzle from $2\pi/9$ rad to 0 rad correlates with an improvement in the results.

Normally, the problems of bacteriological regrowth occur in close contact with the walls, which are the preferred places for bacterial adhesion. Bacterial cells can be removed from the walls by shearing force (Powell and Slater, 1982). Related to this, the wall shear stress magnitude was calculated for the three simulated cases on the walls and the bottom of the tank (T1_1, T2_1 and T3_1 simulations). The maximum value was 0.331 $kgs^{-2}\,m^{-1}$ for T1_1, 0.487 $kgs^{-2}\,m^{-1}$ for T2_1 and 0.177 $kgs^{-2}\,m^{-1}$ for T3_1. Although there were differences on the contours among the three simulated cases (contour shape and location), the maximum values were in the same order of magnitude and there were no significant differences in the range, intensity and distribution of wall shear stresses data.

According to calculated indexes, a good level of mixing is achieved with the prototype T1_1. Inlet changes can induce small changes on the salt dilution in the tank. The best case among the three configurations is T2_1 when considering velocity gradient, dimensionless mixing time and wall shear stress, although T3_1 gives a better result for short-circuit index.

Influence of R_{jet}

Analogous to the previous analysis, in this section a sensitivity analysis of the mixing efficiency is performed for changes of the inflow Reynolds number. A comparison of the calculated mixing parameters for the different inflow cases with T1 configuration is shown in

Table 3.

A comparison between mixing power and velocity gradient for the different inflows in the simulated T1 (T1_0, T1_1, T1_2, T1_3 and T1_4) was carried out and analysed. It is possible to observe how mixing increases with higher inflows (T1_3 and T1_4). No major differences can be observed in the dimensionless mixing time when the inflow increases. The configurations with better mixing performance corresponds to T1_3 and T1_4.

The index θ_{10} was also calculated. All the results are very similar and lower than 0.2, which indicates a poor mixing from a short-circuit point of view. The best case among all the simulated inflows was T1_4 which corresponds to the highest inflow case.

The wall shear stress magnitude was also calculated for the different inflows in T1. The maximum value was 0.052 $kgs^{-2}m^{-1}$ for T1_0, 1.089 $kgs^{-2}m^{-1}$ for T1_2, 1.734 $kgs^{-2}m^{-1}$ for T1_3 and 3.388 $kgs^{-2}m^{-1}$ for T1_4. As was expected, a higher R_{jet} with the same jet diameter induces a higher maximum value of the wall shear stress. Although the magnitude increases with the inflow, the contours of the wall shear stress have the same shape and location. This means that higher R_{jet} can help to solve problems of bacteriological regrowth on the walls.

The best case among the different inflows is T1_4, according to velocity gradient, wall shear stress and short-circuit index; meanwhile T1_3 performs better for dimensionless mixing time.

4 Conclusion and future research

In this paper, the results of three-dimensional numerical simulations have been presented for a drinking water storage tank with constant inflow and outflow. CFD techniques provide information for every cell within the domain and can simulate complex three-dimensional flow structures, mixing and dilution. The paper shows a procedure for the analysis of the mixing processes in water tanks using experimental and computational techniques validated with experimental results.

A high degree of correlation has been achieved between experimental and simulated dilution curves for the initial configuration T1_1. The mixing process and its relation to the different phases of the dilution curve has been studied, showing a predominantly advective transport. By studying the statistics (i.e. histogram tracer concentration) it is possible to see the change of dispersion and position of the tracer values over time, and the point at which the salt concentration averages and the dilution curve stabilises 0.2 gl^{-1}, around 260 s after the brine injection. The results show a good mixing capability of the initial prototype T1_1, achieving a homogeneous mixing of the injection with no significant changes in dispersion parameters after 560 s.

After validation of the experimental case (T1_1 configuration), an analysis of the influence of the horizontal inlet orientation on mixing efficiency is presented. Two configurations, T2_1 and T3_1, are proposed, which are based on a modification of the horizontal angle θ of the jet nozzle (from 0 rad to $2\pi/9$ rad). Changes of R_{jet} are also analysed. The R_{jet} varies between 9,860 to 88,736 (T1_1, T1_2, T1_3 and T1_4). Mixing parameters, such as mixing power P, the velocity gradient G, dimensionless mixing time τ_m and the short-circuit mixing index θ_{10}, are used in this study. A $\varphi = 0$ rad and $\theta = \pi/9$ rad position of the diffuser (case T2_1) shows a slight improvement in the mixing capability in terms of velocity gradient, dimensionless mixing time and wall shear stress, while for a $\varphi = 0$ rad and $\theta = 0$ rad position (case T3_1) mixing capability increases for the mixing index θ_{10}. These results indicate that small modifications of the horizontal inlet angle, generate slight changes in the flow structure and, hence, in the mixing processes. Furthermore, the increase of the inflow discharge for a specific jet orientation and diameter induces an improvement of the velocity gradient and the wall shear stress, although the best case is T1_3 ($Q_{in} = 9.72 \cdot 10^{-4}$ m^3s^{-1}) according to the dimensionless mixing time and T1_4 ($Q_{in} = 1.25 \cdot 10^{-3}$ m^3s^{-1}) for the mixing index θ_{10}.

Future research will focus on extrapolating the technique and applying it. More research must be done in order to predict the changes due to nozzle configurations and to conduct validations with different number of nozzles. CFD techniques in addition with experimental procedures, will be a useful tool for the design, improvement and management of water tanks.

Acknowledgements

This work has been conducted within the framework of the research project "*Línea Multidisciplinar para Aplicación de las técnicas de la Mecánica de Fluidos Computacional a la modelación de movimiento de flujos ambientales (*2614*)*" from *Vicerrectorado de Investigación, Universidat Politècnica de València*, Spain.

Notation

CFD = computational fluid dynamics

COV = coefficient of variation

C_{Salt} = salt concentration (gl^{-1})

D_m = coefficient of molecular diffusion (m^2s^{-1})

F_d = densimetric Froude number

G = velocity gradient (s^{-1})

H = vertical dimension of the tested tank (m)

l = characteristic length scale (m)

L = longitudinal dimension of the tested tank (m)

M = momentum flux of the inflowing jet (m^4s^{-4})

P = mixing power (W)

Pe = Peclet number (-)

Q_{in} = inflow tank (m^3s^{-1})

R_{jet} = Reynolds number in the jet nozzle section (-)

T_r = theoretical residence time (s)

t = time (s)

t_{10} = 10% arrival time (s)

t_m = mixing time (s)

URANS = unsteady Reynolds-average navier-stokes

U = characteristic velocity (ms^{-1})

U_{in} = inlet velocity (ms^{-1})

U_{jet} = jet nozzle velocity (ms^{-1})

$\langle U \rangle$ = mean velocity magnitude (ms^{-1})

$\langle u \rangle$ = longitudinal mean velocity module (ms^{-1})

V_t = volume of the tank (m^3)

$\langle v \rangle$ = transverse mean velocity vector module (ms^{-1})

$\langle w \rangle$ = vertical mean velocity module (ms^{-1})

W = transverse dimension of the tested tank (m)

WDS = water distribution system

X = longitudinal direction of the model (m)

Y = transverse direction of the model (m)

y^+ = dimensionless wall distance (-)

Z = vertical direction of the model (m)

Δp = pressure drop (Pa)

φ = vertical inlet angle (º)

μ = dynamic viscosity (m^2s^{-1})

θ = horizontal inlet angle (º)

θ_{10} = short-circuit index (-)

τ = dimensionless time (-)

τ_m = dimensionless mixing time (-)

References

Boulos, B.F., Altman, T., Jarrige, P.A. & Collevati, F. (1994). A discrete simulation approach for network water quality models. *J. Water Resour. Plng. Mgmt., 121*(1), 49–60.

CD-Adapco, Inc. (2010). STAR-CCM+ (5.04.006) User's Guide. New York, USA.

Gibson, M.M., & Launder, B.E. (1978). Ground effects on pressure fluctuations in the atmospheric boundary layer. *J. Fluid Mech., 86*(3), 491–511.

Clark, R.M., Goodrich, J.A. & Wymer, L.J. (1993). Effect of the Distribution System on the Water Quality. *J. AQUA., 42*(1), 30–38.

Grayman, W.M. & Clark, R.M. (1993). Using computer models to determine the effects of storage on water quality. *J. Am. Water Works Assoc., 85*(7), 67–77.

Grayman, W.M., Deininger, R.A., Green, A., Boulos, P.F., Bowcock, R.W. & Godwin, C.C. (1996). Water quality and mixing models for tanks and reservoirs. *J. AWWA., 88*(7), 60–73.

Grayman, W.M., Rossman, L.A., Deininger, R.A., Smith, C.D., Arnold, C.N. & Smith, J.F. (2004). Mixing and aging of water in distribution system storage facilities. *J.AWWA., 96*(9), 70–80.

Hannoun, I.A. & Boulos, P.F. (1997). Optimizing distribution storage water quality: a hydrodynamic approach. *J. Appl. Math. Modelling, 21*, 495–502.

Kennedy, M.S., Moegling, S., Sarikelle, S. & Suravallop, K. (1993). Assessing the effects of storage design on water quality. *J. Am. Water Works Assoc., 85*(7), 78–88.

Mahmood, F., Pimblett, J.G., Grace, N.O. & Grayman, W.M. (2005). evaluation of water mixing characteristics in distribution system storage tanks. *J. AWWA., 97*(3), 74–88.

Marek, M., Stoesser, T., Roberts, P. J. W., Weitbrecht, V. & Jirka, G. H. (2007). CFD Modeling of turbulent jet mixing in a water storage tank. *XXXII IAHR Congress*, Venice, Italy.

Martínez-Solano, F.J., Iglesias-Rey, P.L., Gualtieri, C. & López-Jiménez, P.A. (2010). Modelling flow and concentration field in rectangular water tanks. *International Congress on Environmental Modelling and Software Modelling for Environment's Sake, iEMSs, Fifth Biennial Meeting*, Ottawa, Canada.

Martínez-Solano, F.J., Mora-Rodríguez, J.J., Iglesias-Rey, P.L. & López-Patiño, G. (2010). Parameters determination for a mixing model in storage facilities in water distribution systems. López-Jiménez et al. (Eds.), *Environmental hydraulics. Theoretical, experimental and computational solutions* (pp. 303–305). Leiden: CRC Press/Balkema.

Maruyama, Y.B. & Mizushina, T. (1982). Jet mixing of fluids in tanks. *J. Chemical Eng. Japan., 15*, 342–348.

Mau, R.E., Boulos, P.F., Clark, R.M., Grayman, W.M., Tekippe, R.J. & Trusell, R.R. (1995). Explicit mathematical models of distribution storage water quality. *J. Hydraulic Eng., 121*, 669–709.

Metcalf & Eddy, Inc. (1995). *Wastewater engineering treatment and reuse*. New York, USA: McGraw-Hill.

Metzger, B. & Westrich, B. (1978). *Mixing and exchange ratios in a clean water tank* (Research Report). Institute for Hydromechanics, University of Karlsruhe, Germany.

Palau-Salvador, G., Weitbrecht, V., Stoesser, T., Bleninger, T., Hofmann, B., Maier, M., Roth, K. (2007). Numerical simulations to predict the hydrodynamics and the related mixing processes in water storage tanks. *Proc. IAHR Congress*, Venice, Italy.

Patwardhan, A.W. (2002). CFD modeling of jet mixed tanks. *Chemical Engineering Science, 57*, 1307–1318.

Powell, M.S., & Slater, N.K. (1982). Removal rates of bacterial cells from glass surfaces by fluid shear. *Biotech. Bioeng., 24*, 2527–2537.

Prešeren, T, Steinman, F, Širok, B. & Bajcar, T. (2013). The theoretical densimetric Froude number values with favourable effect on the clarifier performance. *Chemical Engineering and Processing: Process Intensification, 74*, 97–105.

Rossman, L.A. & Grayman, W.M. (1999). Scale-model studies of mixing in drinking water storage tanks. *J. Environmental Eng., 125*, 755–761.

Rushton, J.H. & Oldshue, J.Y. (1953). Mixing: present theory and practice. *Chem. Eng. Prog., 49*, 161–167.

Shih, T.H., Liou, W.W., Shabbir, A., Yang, Z. & Zhu, J. (1994). *A new k-ε eddy viscosity model for high reynolds number turbulent flows: model development and validation* (NASA TM 106721). USA.

Teixeira, E.C. & Siqueira, R. (2008). Performance assessment of hydraulic efficiency indexes. *J. Environmental Eng., 134*, 851–859.

Tian, X. & Roberts, P.J. (2008). Mixing in water storage tanks. I: No buoyancy effects. *J. Envir. Eng., 134*, 974–985.

Van der Walt, J.J. (2002). *The modeling of water treatment process tanks* (PhD Thesis). Rand Afrikaans University, South Africa.

Van der Walt, J.J. & Haarhoff, J. (2000). Is a reservoir really that simple? A cfd investigation into the internal hydraulics of reservoirs. *Proc. of WISA 2000 Conf.*, Sun City, South Africa.

Veersteg, H.K. & Malalasekera, W. (1998). *An introduction to computational fluid dynamics. The finite volume method*. New York, USA: Longman Scientific and Technical

Yeung, H. (2001). Modelling of service reservoirs. *Journal of Hydroinformatics., 3*, 165–172.

Table 1 Inlet orientation and hydraulics jet parameters of the cases for the simulated tank

	Inflow	Angle of jet nozzle		Jet velocity	Jet Reynolds number
Case	Q_{in} (m^3s^{-1})	θ (rad)	φ (rad)	U_{jet} (ms^{-1})	R_{jet} (-)
T1_1	$4.17 \cdot 10^{-4}$	$2\pi/9$	0	1.90	29,579
T2_1	$4.17 \cdot 10^{-4}$	$\pi/9$	0	1.90	29,579
T3_1	$4.17 \cdot 10^{-4}$	0	0	1.90	29,579
T1_0	$1.36 \cdot 10^{-4}$	$2\pi/9$	0	0.63	9,860
T1_2	$6.94 \cdot 10^{-4}$	$2\pi/9$	0	3.17	49,298
T1_3	$9.72 \cdot 10^{-4}$	$2\pi/9$	0	4.44	69,017
T1_4	$1.25 \cdot 10^{-3}$	$2\pi/9$	0	5.71	88,736

Table 2 Mixing parameters for the preliminary model (T1_1) and the two proposals for the horizontal inlet angle (T2_1 and T3_1)

	Inflow	Mixing power	Velocity gradient	Dimensionless mixing time	Short-circuit
Case	Q_{in} (m^3s^{-1})	P (W)	G (s^{-1})	τ_m	θ_{10}
T1_1	$4.17 \cdot 10^{-4}$	0.961	19.415	8.27	0.0915
T2_1	$4.17 \cdot 10^{-4}$	0.974	19.546	4.90	0.1040
T3_1	$4.17 \cdot 10^{-4}$	0.938	19.187	6.17	0.1041

Table 3 Mixing parameters for the preliminary model (T1) and the simulated inflows

	Inflow	Mixing power	Velocity gradient	Dimensionless mixing time	Short-Circuit
Case	Q_{in} ($m^3\ s^{-1}$)	P (W)	G (s^{-1})	τ_m	θ_{10}
T1_0	$1.36 \cdot 10^{-4}$	0.036	3.760	6.62	0.0930
T1_1	$4.17 \cdot 10^{-4}$	0.961	19.415	8.27	0.0915
T1_2	$6.94 \cdot 10^{-4}$	4.430	41.693	6.85	0.0962
T1_3	$9.72 \cdot 10^{-4}$	12.129	68.992	5.79	0.0967
T1_4	$1.25 \cdot 10^{-3}$	25.750	100.522	5.98	0.0968

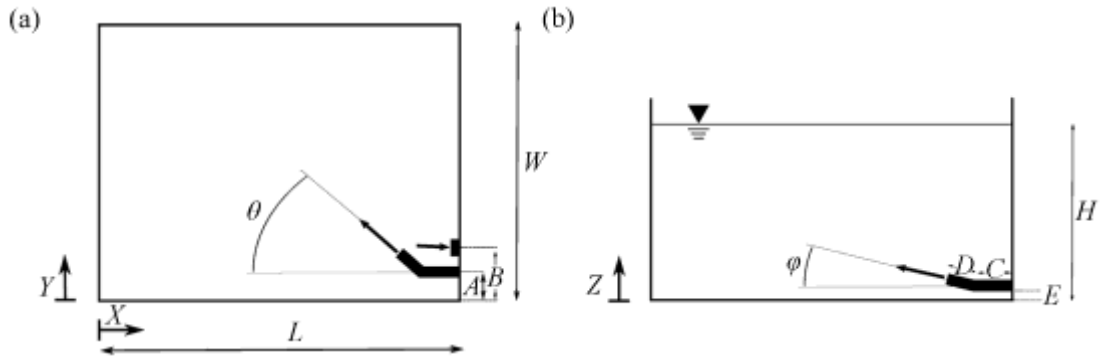

Figure 1 Top (a) and side view (b) of the experimental case used for the simulations. AE: inlet pipe; BE: outlet pipe

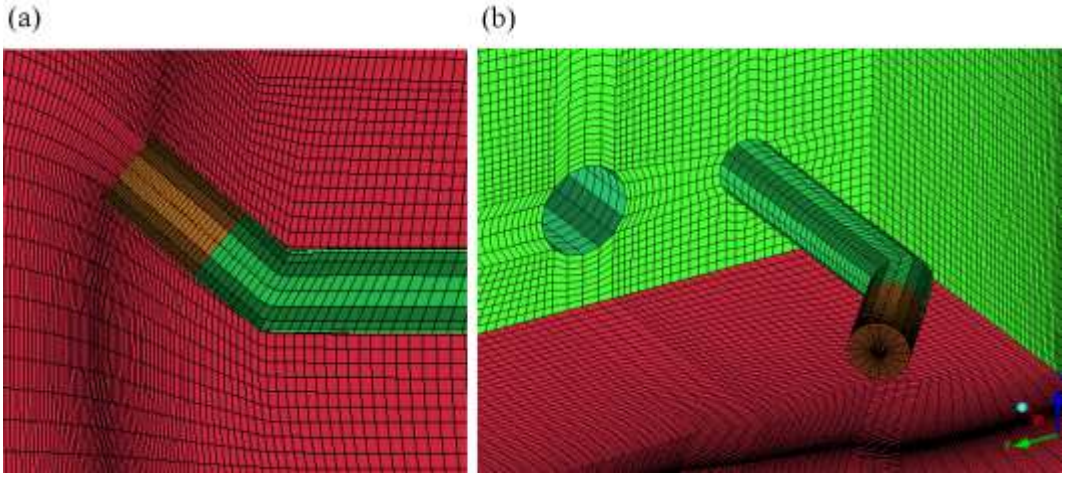

Figure 2 Views of the inlet and outlet structured mesh in the tank (T1 case). Left: top view; right: perspective view

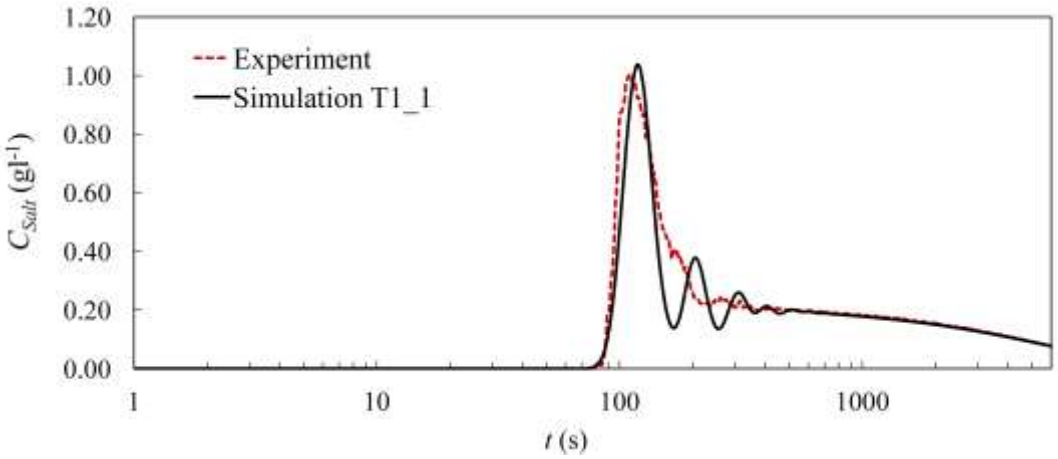

Figure 3 Salt concentration in the outlet section for T1_1 simulation (continuum line) with the experimental results for T1_1 (dotted lines)

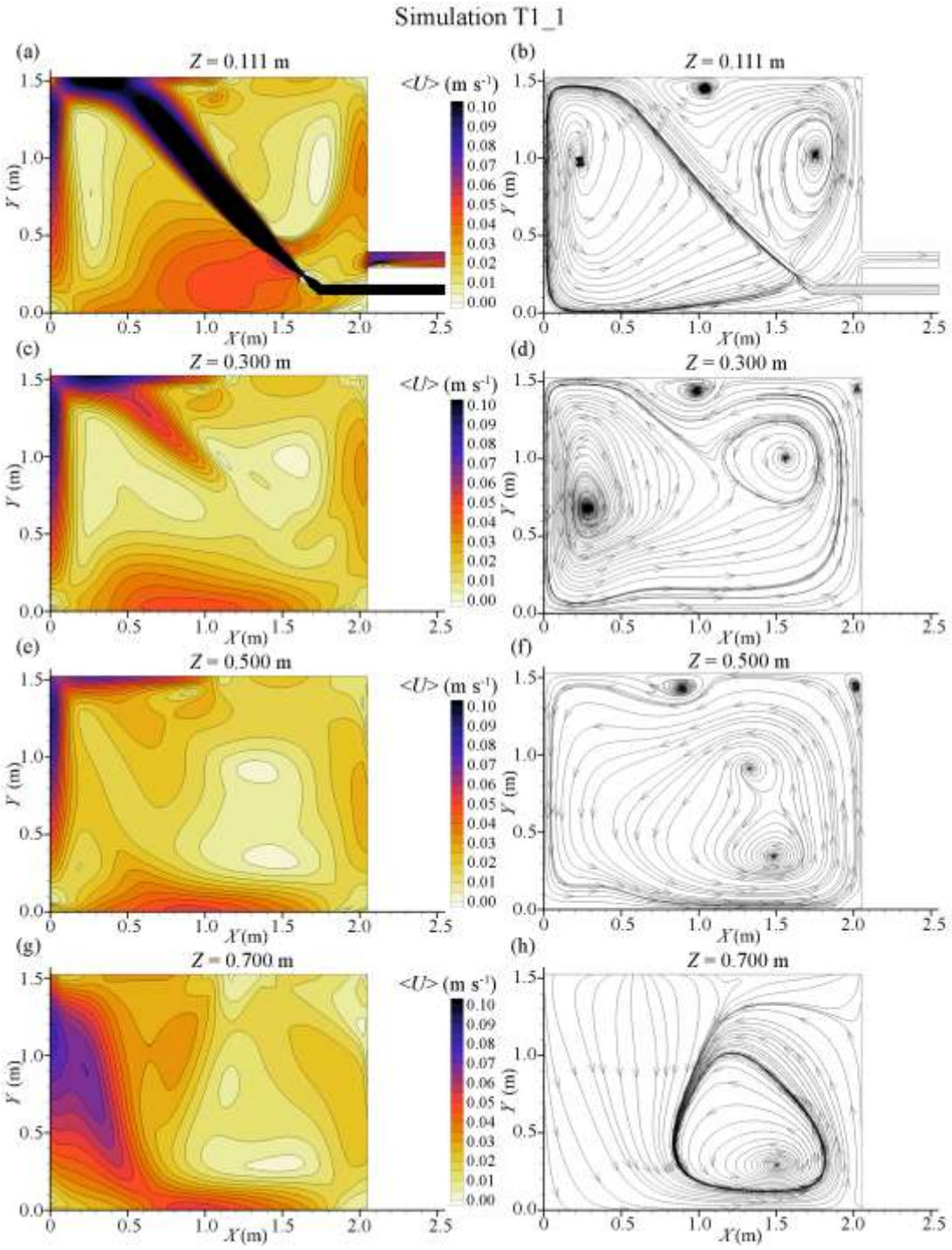

Figure 4 Horizontal sections of simulated mean flow results (T1_1 case). Left: contours of mean velocity vector module $\langle U \rangle = \sqrt{\langle u \rangle^2 + \langle w \rangle^2 + \langle v \rangle^2}$. Right: streamlines of mean flow in four different sections in the tank

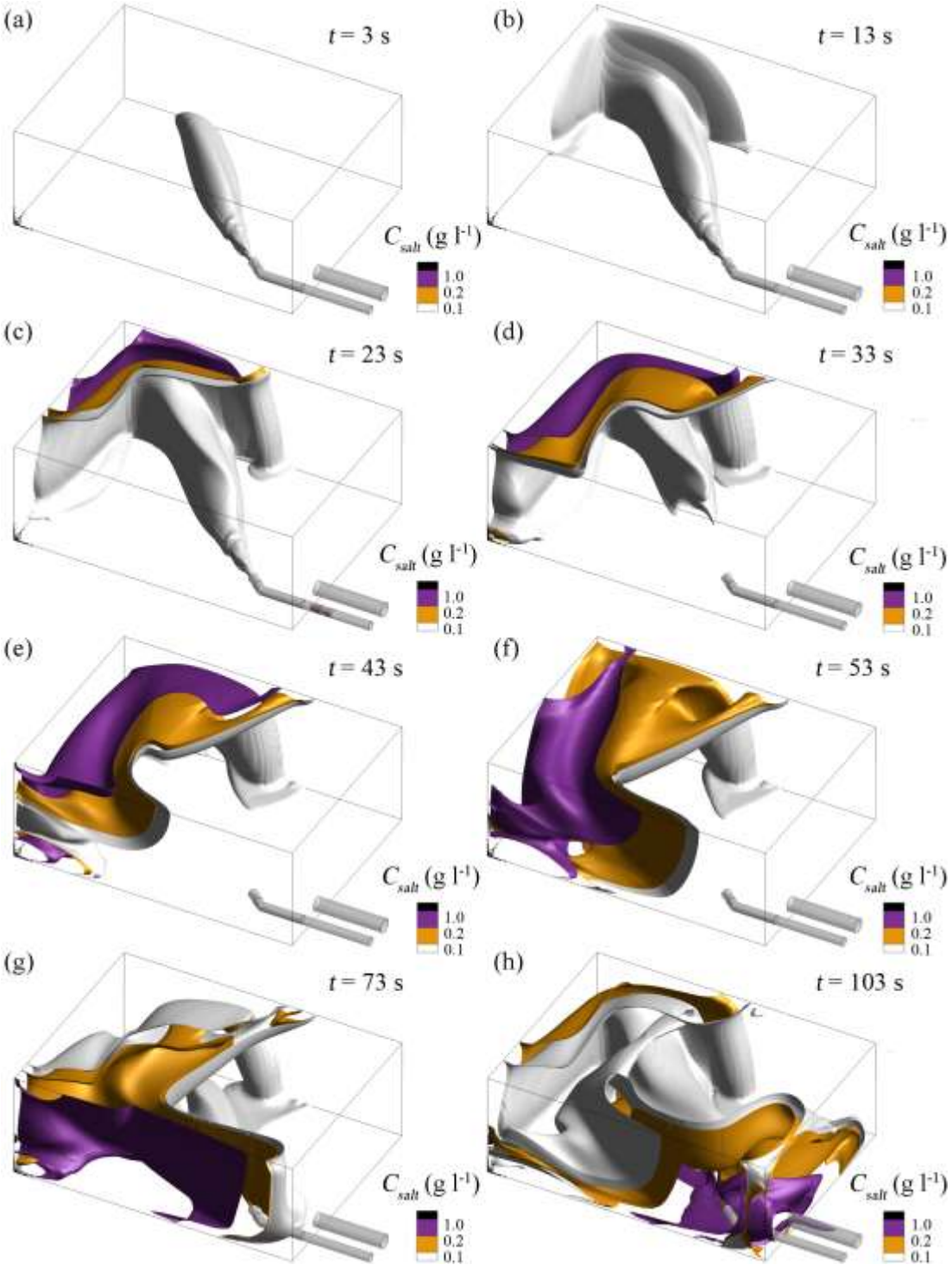

Figure 5 Different views at different specific times (t = 3 s to t = 103 s) of the salt concentration iso-surfaces (1g l^{-1}; 0.2 g l^{-1} and 0.1 g l^{-1}) for T1_1 simulation

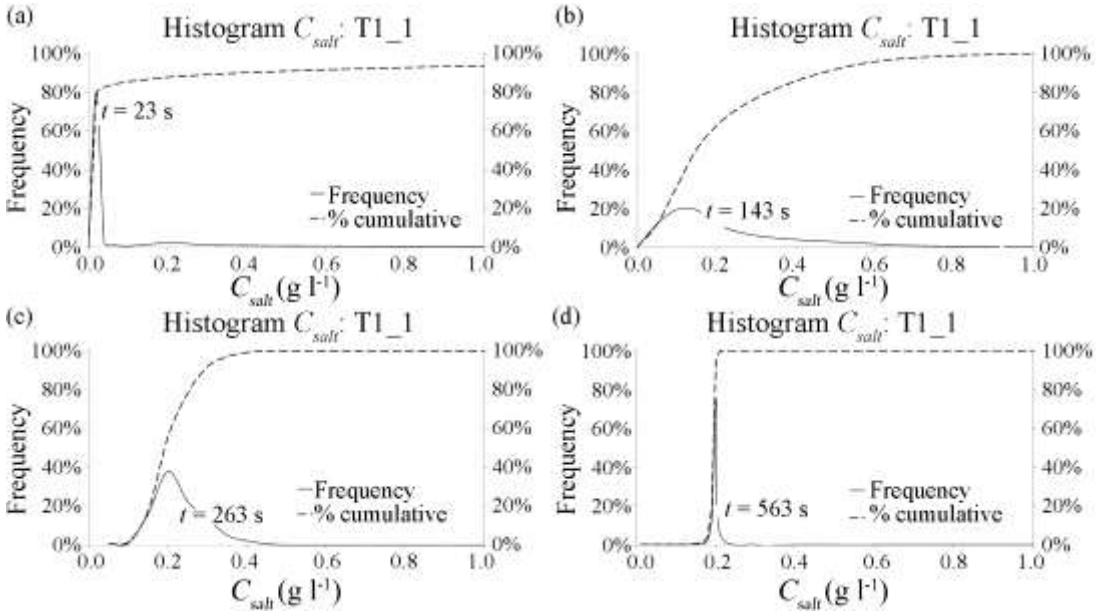

Figure 6 Histogram of tracer concentration C_{Salt} for simulation T1_1 (main axis: histogram of concentration; secondary axis: cumulative histogram of concentration) at different times from the tracer injection

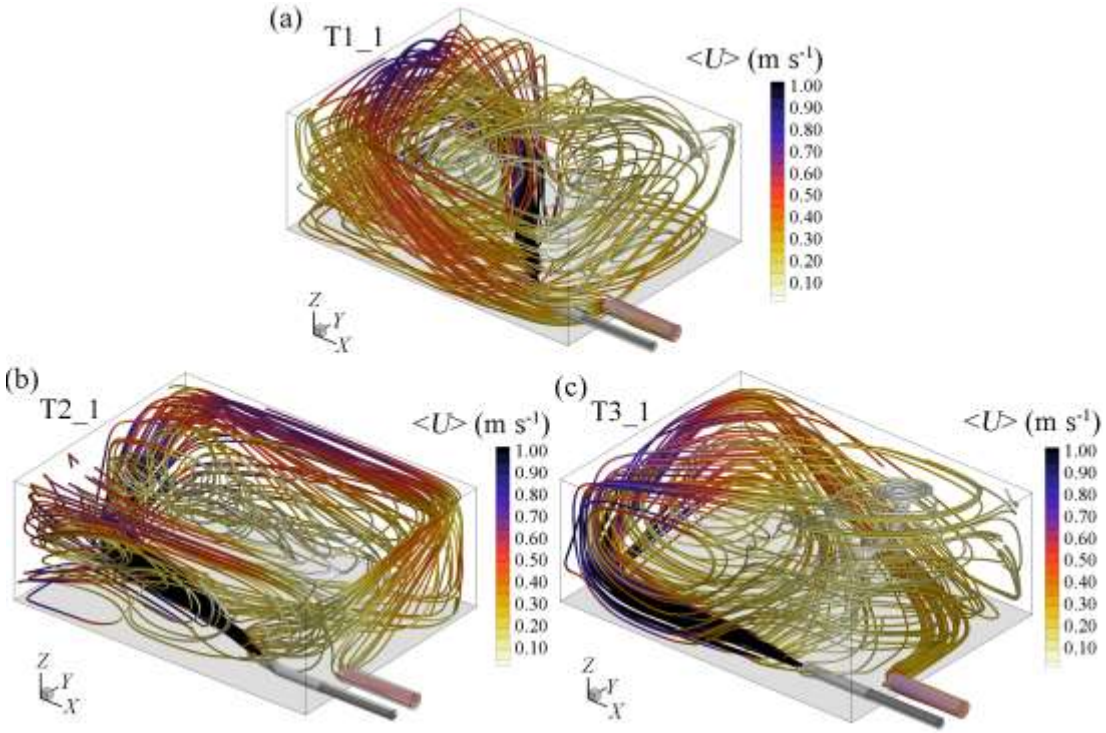

Figure 7 Views of the simulated three dimensional mean flow field (T1_1 simulation, T2_1 simulation, T3_1 simulation): streamlines coloured by the mean velocity vector module $\langle U \rangle$ ($\langle U \rangle = \sqrt{\langle u \rangle^2 + \langle w \rangle^2 + \langle v \rangle^2}$)